Analyzing the Effect of Intraseasonal Meteorological Variability and Land Cover on Aerosol-Cloud Interactions during the Amazonian Biomass Burning Season

J. E. Ten Hoeve[1], L. A. Remer[2], and M. Z. Jacobson[1]

[1]{Department of Civil and Environmental Engineering, Stanford University, CA, USA}

[2]{NASA Goddard Space Flight Center, Greenbelt, MD, USA}

Correspondence to: J. E. Ten Hoeve (tenhoeve@stanford.edu)

Abstract

High resolution aerosol, cloud, water vapor, and atmospheric profile data from the Moderate Resolution Imaging Spectroradiometer (MODIS) are utilized to examine the impact of aerosols on clouds during the Amazonian biomass burning season in Rondônia, Brazil. It is found that increasing background column water vapor (CWV) throughout this transition season between the Amazon dry and wet seasons exerts a strong effect on cloud properties. As a result, aerosol-cloud correlations should be stratified by column water vapor to achieve a more accurate assessment of the effect of aerosols on clouds. Previous studies ignored the systematic changes to meteorological factors during the transition season, leading to possible misinterpretation of their results. Cloud fraction is shown generally to increase with aerosol optical depth (AOD) for both low and high values of column water vapor, whereas the relationship between cloud optical depth (COD) and AOD exhibits a different relationship. COD increases with AOD until AOD ~ 0.25 due to the first indirect (microphysical) effect. At higher values of AOD, COD is found to decrease with increasing AOD, which may be due to: (1) the inhibition of cloud development by absorbing aerosols (radiative effect) and/or (2) a retrieval artifact in which the measured reflectance in the visible is less than expected from a cloud top either from the darkening of clouds through the addition of carbonaceous biomass burning aerosols or subpixel dark surface contamination in the measured cloud reflectance. If (1) is a contributing mechanism, as we suspect, then a linear relationship between the indirect effect and increasing AOD, assumed in a majority of GCMs, is inaccurate since these models

do not include treatment of aerosol absorption in and around clouds. The effect of aerosols on both column water vapor and clouds over varying land surface types is also analyzed. The study finds that the difference in column water vapor between forest and pasture is not correlated with aerosol loading, supporting the assumption that temporal variation of column water vapor is primarily a function of the larger-scale meteorology. However, a difference in the response of cloud fraction to increasing AOD is observed between forest and pasture. This suggests that dissimilarities between other meteorological factors, such as atmospheric stability, are likely to have an impact on aerosol-cloud correlations between different land-cover types.

1 Introduction

The effect of aerosol particles on the hydrological cycle remains one of the largest uncertainties in our climate system. Biomass burning, from both deforestation and annual agricultural burning, is the largest anthropogenic source of such particles in the Southern Hemisphere. A variety of observational and modeling studies have examined the effect of aerosols on the regional hydrometeorology over the Amazon Basin during the biomass burning season (Kaufman and Nakajima 1993, Kaufman and Fraser 1997, Koren et al. 2004, Feingold et al. 2005, Yu et al. 2007, Koren et al. 2008, Zhang et al. 2008, Martins et al. 2009). In these, and in other studies, biomass burning aerosols have been shown to affect clouds through both microphysical and radiative mechanisms (Kaufman et al. 2005b, Kaufman and Koren 2006, Koren et al. 2008, Rosenfeld et al. 2008). Depending on the concentration of aerosol, its chemical composition, size distribution, vertical distribution relative to clouds, and background cloud characteristics, biomass burning aerosols are suggested either to inhibit or invigorate cloud formation and/or growth (Feingold et al. 2005, Koren et al. 2008, Chand et al. 2009).

Carbonaceous biomass burning aerosols can absorb solar radiation, warming the aerosol layer and reducing the radiation reaching the surface (Ackerman et al. 2000, Kaufman et al. 2002, Koren et al. 2004). This effect cools the surface, stabilizes the lower troposphere, suppresses surface heat and moisture fluxes, and slows the hydrological cycle (Jacobson 2002, Andreae et al. 2004, Ramanathan et al. 2005). Evaporation of clouds within the aerosol layer may also occur due to the increase in temperature and decrease in relative humidity caused by aerosol absorption of solar radiation (Yu et al. 2002, Jacobson 2006). Referred to as absorptive

effects or the semi-direct effect, these radiative processes primarily suppress the formation and growth of clouds.

Microphysical effects, on the other hand, enhance cloud formation and growth. Biomass burning aerosols are hygroscopic and can serve as cloud condensation nuclei (Feingold et al. 2001, Andreae et al. 2002, Andreae et al. 2004). Expansion chamber experiments have shown that the addition of cloud condensation nuclei nucleates a larger number of smaller cloud droplets, and these droplets are therefore slower to coalesce to form precipitation (Gunn and Phillips 1957, Squires et al. 1958). These aerosol processed clouds are also more reflective, change drizzle properties, and have been suggested to have longer lifetimes (Twomey 1977, Albrecht 1989). However, the apparent darkening of clouds by absorptive biomass burning aerosols has also been observed by satellite (Kaufman and Nakajima 1993, Wilcox et al. 2009). Recent studies have shown that these polluted clouds may become invigorated, with higher liquid or ice water paths and cloud top pressures (Andreae et al. 2004, Khain et al. 2005, Koren et al. 2005, Lin et al. 2006, Koren et al. 2008, Rosenfeld et al. 2008, Meskhidze et al. 2009). The delay of raindrop formation in polluted clouds suppresses downdrafts, which allows for the generation of greater updrafts and stronger convection. The updrafts carry water vapor to higher altitudes, where additional energy from the latent heat of freezing may be released, further invigorating convection (Williams et al. 2002, Andreae et al. 2004, Rosenfeld et al. 2008). Increases in aerosol optical depth have also been linked to increases in cloud fraction, particularly at low AODs (Koren et al. 2005, Lin et al. 2006, Myhre et al. 2007, Yu et al. 2007).

More recent studies have illustrated that there may be a smooth transition between these competing microphysical and radiative effects (Koren et al. 2008, Rosenfeld et al. 2008). Using MODIS data over the Amazon, Koren et al. (2008) hypothesizes that microphysical processes dominate at lower AODs, increasing cloud fraction and height, whereas radiative processes dominate at higher AODs, decreasing cloud fraction and height. The study also shows that the relative contributions of the microphysical and radiative effects are strongly tied to the initial cloud fraction – the radiative absorption effect begins to dominate at lower values of AOD for lower initial cloud fractions. This is due to the hypothesized aerosol absorption cloud fraction feedback (AFF): Stabilization of the near-surface atmosphere due to aerosol absorption of radiation initially reduces cloudiness, which then exposes more of the aerosol layer, further reducing cloudiness (Koren et al. 2008). Eventually, the reduction in

cloudiness will allow sufficient surface heating to destabilize the lower atmosphere and reverse the positive feedback (Koren et al. 2008). This reduction in cloudiness has also been described as a BC-low cloud positive feedback loop (Jacobson 2002). For low cloud fractions, more of the aerosol layer is available for absorption, resulting in a stronger feedback. For higher cloud fractions, microphysical invigoration will dominate for the same degree of aerosol loading. An implication of this finding is that aerosol effects on either sparse or dense cloud fields may have entirely opposite effects on climate forcing.

For the majority of observational biomass burning studies over the Amazon, the months of August, September, and October are customarily selected due to the combination of high aerosol loading from biomass burning and consistent dry conditions present during these months. The Amazon dry season occurs during the southern hemisphere winter, and is defined by a subtropical high pressure that moves from the Atlantic Ocean over the Amazon Basin (Nobre et al. 1998). Felled vegetation is allowed to dry out during the season, and is burned during the southern hemisphere spring. High pressure typically remains over the region until mid-to-late October, when the onset of the rainy season begins (Nobre et al. 1998). During this biomass burning transition season, cloud properties are assumed to be weakly dependent on meteorology due to the stationary high pressure overhead (Kaufman and Nakajima 1993, Koren et al. 2004, Yu et al. 2007, Koren et al. 2008). However, this study illustrates that gradually increasing background column water vapor (CWV) during the biomass burning transition season, between the end of the dry season and the beginning of the wet season, has a discernable impact on aerosol-cloud correlations.

Previous studies have noted that aerosol loading and CWV are weakly spatially correlated over the Amazon Basin on seasonal timescales (Feingold et al. 2001). On smaller spatial and temporal scales, latitudinal variation of both CWV and AOD will produce high correlations in some areas (Kaufman and Fraser 1997). Regions where simultaneous advection of these two parameters takes place also exhibit high correlations (Remer et al. 1998). However, these studies do not take into consideration inconsistent sampling resulting from temporal correlations on longer intraseasonal timescales. Variability in the CWV, which can be observed from space on high temporal and spatial scales using the MODIS sensor, may be used as a tracer for large-scale meteorological variability. Attempts to remove the influence of meteorology from aerosol-cloud correlations are common; a study by Koren et al. (2005) accounts for meteorology by stratifying data by vertical wind velocity, an NCEP parameter

that correlates well with MODIS cloud parameters. Here, we use column water vapor, which is shown also to correlate well with MODIS cloud parameters, to stratify the aerosol and cloud data.

The latter portion of the paper tests the assumptions made in the former portion of the paper by analyzing effects of aerosols on clouds and column water vapor over different land surface types. Many studies have probed the local effects of deforestation on local and regional meteorology; however no observational studies have analyzed the aerosol effect on clouds over both forested and deforested land. It is estimated that 50% to 60% of total rainfall in the Amazon is derived from evapotranspiration (Marques et al. 1977, Salati and Nobre 1991). Regional modeling studies have estimated a reduction in evapotranspiration of about 30% over deforested regions of the Amazon compared with forested regions (Nobre et al. 1991). A group of studies has probed into the regional climate effects of deforestation through changes in surface energy and water vapor fluxes and land-atmosphere interactions (Henderson-Sellers and Gornitz 1984, Nobre et al. 1991, Cutrim et al. 1995, Wang et al. 2000, Roy et al. 2002, Negri et al. 2004, Wang et al. 2009). Depending on the structure and scale of the deforestation, contrasting effects on clouds and precipitation are observed (D'Almeida et al. 2007). Smaller scale deforestation (i.e. the fish bone pattern) spawns mesoscale circulations that arise from land surface heterogeneities on the finer scale (Segal et al., 1988, Wang et al. 2000, Roy et al. 2002, Wang et al. 2009). Enhanced shallow convection over deforested regions is caused in part by a land breeze from nearby moisture-rich forests. When this moist land breeze reaches unstable air over the deforested region (due to greater surface heating), it rises to form clouds (Segal et al. 1988, Roy et al. 2002). Several observational studies have shown an increase in shallow convection over disturbed regions of the Amazon due to this direct thermal circulation, particularly in the state of Rondônia, Brazil (Cutrim et al. 1995, Negri et al. 2004, Wang et al. 2009). This study differs from previous studies in that the aerosol effect on water vapor and clouds over forested and deforested is examined, a logical extension of the studies noted above.

Accounting for meteorological variability in observational aerosol-cloud correlation studies is paramount. The aerosol effect on cloud properties over the Amazon has been shown to differ in a humid year compared to a dry year (Yu et al. 2007). In the humid year, cloud fraction predominantly increases with increasing AOD, whereas in a dry year, cloud fraction predominantly decreases with AOD. The mechanisms behind this difference are still largely

unexplained (Yu et al. 2007). This study incorporates both dry and wet years, reducing this interannual variability, while also stratifying the data by CWV to ensure similar background moisture conditions exist along the range of AOD retrievals used. This study probes into two primary questions: (1) how can contamination from meteorological variability in observed aerosol-cloud relationships be reduced and (2) what is the aerosol effect on clouds and column water vapor over different land surface types.

2 Data and Methods

MODIS, onboard the Terra and Aqua satellites, provides relatively high spatial resolution (250 m – 500 m) while achieving near global coverage on a daily basis (Salomonson et al. 1989). The Terra satellite is on a sun synchronous orbit with an overpass at approximately 10:30 AM local time, whereas the Aqua satellite overpasses at approximately 1:30 PM local time. The Aqua pass is chosen over the Terra pass since warm clouds are more likely to be developed in the afternoon compared to the morning. We choose MODIS over other sensors, such as the Multi-angle Imaging Spectroradiometer (MISR), due to its high resolution and because MODIS produces a variety of cloud and atmospheric profile products, which other sensors do not (Diner et al. 1998). This study employs MODIS Swath Level 2 aerosol, cloud, water vapor, and stability products (King et al. 2003). Aerosol optical depth from the aerosol product is calculated over land and ocean at a wavelength of 550 nm, with a footprint of 10 km x 10 km (Kaufman et al. 1997, Remer et al. 2005, Levy et al. 2007). Surface reflectances utilized in the aerosol algorithm are dynamic, and related to empirical functions which match reflectances in the near IR to visible wavelengths in order to calculate an NDVI-like measure of vegetation and geometry (Levy et al. 2007). Validation with ground-based AERONET observations yield an overall error of $\pm 0.05 \pm 0.15\tau_a$ over land, where τ_a is the aerosol optical depth at 550 nm (Levy et al. 2007).

The Level 2 cloud product produces retrievals of cloud fraction, cloud top properties, cloud phase properties, and cloud microphysical properties, calculated using fourteen of the thirty-six MODIS spectral bands (Ackerman et al. 1998). The cloud fraction and cloud top properties are produced at 5 km x 5 km resolution, whereas the microphysical properties are produced at 1 km x 1 km resolution (Platnick et al. 2003). The 5 km cloud fraction product is computed using the fraction of 1 km cloudy pixels in the 5 km footprint, as determined by the cloud mask product (Platnick et al. 2003). The cloud mask product is based on the principle

that clouds are characterized by higher reflectance and lower temperature than the earth's surface, and is clear-sky conservative (Ackerman et al. 1997). The cloud phase retrieval is determined by analyzing the contrasting effects of water droplets and ice crystals on the brightness temperature in the infrared bands (Platnick et al. 2003).

The cloud microphysical properties include cloud optical depth (thickness), cloud effective radius, and cloud liquid water path. Cloud optical depth (COD) is inversely calculated from spectral reflectance measurements and surface albedo data by using a lookup table (Nakajima and King 1990, Twomey and Cocks 1982, Twomey and Cocks 1989). For over-land retrievals, COD is calculated at wavelengths 0.645 μm and 2.130 μm. The 1 km and 5 km cloud data are averaged into 10 km x 10 km grid boxes in order to conform to the Level 2 aerosol data.

Column water vapor (precipitable water vapor) is derived by integrating the 101 levels at which water vapor mixing ratios are calculated in the MOD07 atmospheric profile product (Seemann et al. 2002). Units are reported in centimeters of equivalent liquid water. We choose not to use the near-IR column water vapor product due to its limitations over dark surfaces (Gao and Kaufman 1998). The profile algorithms are based on thermal emissions of atmospheric gases with uniform distributions, such as oxygen and carbon dioxide (Seemann et al. 2002). The 1000 hPa temperature is calculated using the skin temperature, surface pressure, and Poisson's Equation for potential temperature. Skin temperature is not the best approximation for surface air temperature; however, for the purposes of finding relative differences in atmospheric stability across our study domain, we feel this is our best option considering that a high-resolution observational temperature data set is currently not available from any other source. The water vapor and profile products are also produced at 5 km resolution, but are averaged to the 10 km scale to conform to the Level 2 aerosol data. Products requiring a clear sky, such as the MOD07 products, are able to be estimated for a majority of 10 km pixels with cloud fractions less than one.

In the first portion of the paper, aerosol and cloud data over all non-water surfaces are included in the analyses. In the latter portion of the paper, MODIS aerosol, cloud, stability, and water vapor data are stratified by land cover type. This requires an up-to-date, high-resolution land cover classification data set. The Land Processes Distributed Active Archive Center (LP DAAC), located at the U.S. Geological Survey (USGS) Earth Resources Observation and Science (EROS) Center, provides a combined Terra/Aqua yearly land cover

product - MCD12Q1 (http://lpdaac.usgs.gov). This product employs MODIS BRDF-adjusted surface reflectances, land surface temperature data, enhanced vegetation index data, and terrain elevation information along with neural network classification algorithms and training data to assign land cover classifications (Strahler et al. 1999). The data are resampled from 500 m x 500 m resolution to 0.1° x 0.1° resolution to approximately match the resolution of the Level 2 swath aerosol, cloud and profile data.

Our 5° x 5° study region encompasses the deforested region of Ji Paraná in Rondônia, Brazil, as well as a protected forest to the east, illustrated in Fig 1. Green regions represent primary forest and yellow regions represent pasture. Blue regions represent land cover classes that do not explicitly fall in either class. Broad-leaf forest classifications are assigned to the forested category, whereas closed shrublands, open shrublands, woody savannas, savannas, grasslands, croplands, cropland and natural vegetation mosaic, and barren or sparsely vegetated classifications are assigned to the pasture category, according to the International Geosphere-Biosphere Programme categorization scheme (Strahler et al. 1999). The percentage of pasture increases with time in our fixed study region due to ongoing deforestation.

A small region is chosen for this study, compared with other studies of its type, so that meteorological differences due to spatial variation will be better removed, and so that stratification of atmospheric data by land cover type can be conducted. The high spatial resolution of the Level 2 data allows for the accumulation of a sufficient data record for analysis, while also reducing the pixel size in which aerosol and cloud characteristics need to be assumed constant. Previous studies have relied on Level 3 data, which assumes aerosol and cloud characteristics are constant over 1° x 1° pixels (Koren et al. 2008). The study encompasses the Amazonian biomass burning months of August, September and October for the years 2004 through 2007. This time period includes both dry and wet years, as well as years with both heavy and light biomass burning, according to MODIS and NCEP/NCAR Reanalysis data (Kalnay et al. 1996, Koren et al. 2007). The inclusion of multiple years of data reduces the interannual variability present in the data. In addition, using multiple years allows for the compilation of a large enough data set for analysis in the small study region.

To account further for meteorological variability, NCEP/NCAR Reanalysis 700 hPa wind vectors are used to remove days for which the South Atlantic Subtropical High was not the dominant weather pattern over the region (Kalnay et al. 1996). This resulted in a removal of 43 days over the four year period, equaling 12% of the total number of days in the months of

August through October in 2004 through 2007. All retrievals that are not considered "useful" or were considered "bad" quality according to the Level 2 quality assurance bit data were also removed. Warm clouds are segregated from cold and unknown-phase clouds by only retaining 10 km pixels that contain >95% of 1 km cloud retrievals in the liquid water phase. The re-sampled 10 km atmospheric aerosol, cloud, and profile data are then segregated by forest and pasture in the latter portion of the paper to explore the effect of land-atmosphere-aerosol interactions on CWV and clouds.

Aerosol optical depth and column water vapor MODIS satellite retrievals are compared with Aerosol Robotic Network (AERONET) sun photometer data in Fig S1 (Holben et al. 1998). Data represent two stations within the 5° x 5° study region, Abracos Hill, active in 2004 and 2005, and Ji Paraná SE, active in 2006 and 2007. Only days used in the study are included. Correlation coefficients between MODIS and AERONET retrievals are above 0.90 for both aerosol optical depth and column water vapor, providing confidence in the MODIS satellite retrievals.

3 Results

3.1 Effect of Intraseasonal Meteorological Variability

CWV increases over our study region throughout the dry-to-wet transition season between the months of August to October. Fig 2a shows MODIS CWV and liquid water cloud fraction averaged into eight equally-spaced bins between August 1st and October 31st, for all years between and including 2004 and 2007. Cloud fraction and CWV are understandably highly positively correlated, as water vapor is one of the principal components required for cloud formation. Fig 2b shows MODIS aerosol optical depth at 550 nm, also binned by day of the season, similar to Fig 2a. Unlike CWV, AOD increases from August 1st until approximately the middle of September, at which point the trend reverses and decreases until the end of the season on October 31st. This mid-season peak in aerosol loading is indicative of a biomass burning peak that is largely determined by social behavior. Burning customarily occurs late enough into the season to sufficiently allow vegetation to dry out, but not too late to risk an early onset of the rainy season.

Fig 2 indicates that CWV and cloud fraction are directly correlated with aerosol optical depth during the first half of the season, whereas these variables are inversely correlated during the

second half of the season. Thus, if we plot CWV and cloud fraction directly against AOD, separated into the two halves of the season, we would expect the signs of the regression slopes to be the same for each parameter in each half season. If CWV increases with aerosol in the first half season, then so should cloud fraction. If CWV and AOD are negatively correlated in the second half season, then cloud fraction should also be negatively correlated with AOD.

Fig 3a shows CWV binned by aerosol optical depth for all non-zero cloud fraction retrievals in our study region for the same time period as in Fig 2. The data are stratified by day of the season, with plots representing each half of the season and all days in the season. Fig 3b depicts liquid cloud fraction binned by aerosol optical depth, for the same periods as in Fig 3a. In these figures, cloud properties and CWV are binned by AOD, with each bin representing 12.5 percentile of the AOD values. This method has been used previously in other studies so that bias is not introduced through inconsistent sampling in each bin (Lin et al. 2006). The absolute low and high AOD boundaries are assigned to be 0.05 and 0.8, however, the location of individual bin edges vary for each plot. The bin centers are defined as the average AOD value in each bin. Error bars representing the standard errors of the bin average ($\sigma/N^{1/2}$) are included for each bin. Because the number of samples is equal for each bin due to the sampling procedure used, the standard error is directly proportional to the standard deviation of the samples in each bin.

Even though AOD values greater than 0.8 are routinely observed in this region during the biomass burning season, higher values are not included to prevent aerosol misclassification as cloud (Brennan et al. 2005). In this range, significant cloud contamination of aerosol by clouds is also unlikely, yet occasional contamination may still occur (Kaufman et al. 2005b). It is also improbable that these correlations are due to a 3D cloud effect, which artificially increases AOD retrievals in the regions neighboring clouds (Wen et al. 2006). This effect has been shown to be larger for greater cloud cover and aerosol loading, but our results indicate that the strongest positive correlation between cloud fraction and AOD occurs at low AODs (Yu et al. 2007). It is also unlikely that the positive cloud fraction-AOD correlation is due to atmospheric stability, since increasing AOD has been shown to correlate with increasing stability (Davidi et al. 2009).

In the first half season, Aug. 1st to Sep. 15th, there is a positive correlation between both CWV and AOD, as well as between cloud fraction and AOD, as expected from Fig 2. However, in

the second half season, Sept. 15th to Oct. 31, the CWV is negatively correlated with AOD as expected, but cloud fraction is not. This deviation of the cloud fraction relationship to AOD in a direct correlation overrides the controlling effect of the seasonal CWV evolution on cloud formation and strongly points to aerosol as a modifying element of cloud properties. We conclude that both large-scale meteorological factors traced by seasonally varying CWV and aerosol loading contribute to changes in water cloud fraction in our region of interest.

This conclusion has important implications for aerosol-cloud analysis. Following previous studies, common practice would be to accumulate all pixels with both aerosol and cloud retrievals during the August-October season, and then bin the cloud retrievals by aerosol optical depth, implicitly assuming constant meteorological conditions throughout this period (Koren et al. 2004, Yu et al. 2007, Koren et al. 2008). However, this study finds that embedded in these correlations are systematic variations in CWV with aerosol optical depth. As a result, this intraseasonal CWV signal may impact aerosol-cloud correlations. For example, the "boomerang" shape identified by Koren et al. (2008) and attributed to the combination of microphysical and radiative effects by aerosols on clouds may also contain an element of intraseasonal evolution of the meteorological conditions. In Fig 3a we identify a boomerang shape in the CWV vs. AOD plot that is due solely to the combination of the different halves of the season, and not a physical consequence of the aerosol at all. The similar boomerang shape in cloud fraction over the full biomass season seen in Fig 3b reflects both the actual relationship between cloud fraction and aerosol in the latter half season and also the artifact created by combining the two half seasons.

Fig 3c and Fig 3d show CWV and cloud fraction again binned by AOD, but only for cloud fractions less than 0.5. By retaining only low cloud fractions, more of the aerosol layer is exposed to sunlight in each 10 km x 10 km retrieval box. In these scenes, it has been hypothesized that the increased aerosol exposure to sunlight will result in a stronger absorption effect on clouds and that the decrease of cloud fraction with AOD will begin at lower values of aerosol loading (Koren et al. 2008). The lower cloud fraction should not affect the relationship between CWV and AOD, because CWV should not be affected by a warming atmospheric column. Indeed, Fig 3c shows little difference in both the shape of the graph and the magnitude of the change of CWV with AOD when compared with Fig 3a.

Exposure to sunlight has little effect on column water vapor. However, consistent with Koren et al. 2008, we find that exposure to sunlight does affect the relationship between aerosol

loading and cloud fraction. The less cloudy plot of Fig 3d has shifted the turning point between increasing and decreasing cloud fraction to lower aerosol loading. Fig 3d locates the turning point at AOD = 0.30, as opposed to the total data set of Fig 3b where the turning point is at AOD = 0.55.

Fig 2 and Fig 3 both confirm the associations between clouds and aerosols identified from satellite retrievals seen in previous studies and also sound a warning that some of these associations contain an artifact introduced from slowly evolving meteorological factors that can be traced by CWV. We note a difference between this study and the previous studies mentioned above. We are focusing on a very small (5^{o} by 5^{o}) box in Rondônia, and previous studies took a broader view that included the entire Amazon Basin with its varied surface types, biomes and climatic zones. The trends shown in Fig 2 are applicable for larger areas as well, but the range between low and high CWV and low and high AOD over the season becomes diluted as the study area is expanded. Our study area captures the strong seasonal variation in water vapor, cloud and aerosol properties that still exists but in diluted magnitudes when our region is combined with the surrounding areas. **(So, as the study area is expanded, the range of CWV and AOD values decreases? This is confusing to me)**

We can identify intraseasonal meteorological variations by using CWV as a tracer for the slow onset of the rainy season and stratify the data set using this parameter to control for meteorology. Fig 4a depicts CWV binned by AOD for all cloud fraction retrievals, and for five percentile groupings of CWV. Each grouping spans 16 percentile points, with a minimum percentile of 10% and a maximum percentile of 90% to avoid outlier values. These bounding low and high percentiles refer to CWV values of 2.10 cm and 5.33 cm, respectively. In general, the lower percentiles represent retrievals early in the season whereas higher percentiles represent retrievals late in the season. In each grouping, CWV only varies marginally between AOD bins, with a maximum difference of 0.09 cm between any two bins in any grouping. This nominal variation in CWV within each grouping is likely to have only a minimal effect on cloud properties.

Fig 4b depicts cloud fraction binned by AOD for the five CWV groupings. The change in cloud fraction with AOD in Fig 4b is more representative of the true aerosol effect on cloud fraction compared to Fig 3 since the influence of varying CWV has been minimized. For each CWV grouping, cloud fraction either exhibits a modest increasing trend, on average, across the AOD range between 0.05 and 0.8, or remains relatively constant along this range.

The 42nd to 58th percentile grouping and the 58th to 74th percentile groupings do not exhibit an increasing trend to the extent of the other groupings. The difference in the aerosol effect on cloud fraction does not appear to be largely dependent on CWV, which agrees with previous studies (Feingold et al. 2001).

In general, cloud fraction appears to increase with AOD at the greatest rate at low AODs, specifically for the lowest CWV grouping as well as the highest CWV grouping. The highest CWV group, the 74th to 90th percentile, demonstrates the greatest microphysical effect - cloud fraction increases at the greatest rate below an AOD of 0.35 compared to other groupings. **In high water vapor loading environments with low cloud condensation nuclei, addition of aerosol may increase cloud fraction to a greater extent than in lower water vapor loading environments due to the impact of stronger updrafts on the lifetime effect (Albrecht 1989, Kaufman and Fraser 1997) (Can I say this?).** This result also agrees with the aerosol absorption cloud fraction feedback – the greater the initial cloud fraction, the greater the microphysical effect (Koren et al. 2008). The flattening of these curves at higher AODs suggests a saturation of the microphysical effect. The absence of an aerosol absorption effect in Fig 4b conflicts with some studies (Koren et al. 2004, Koren et al. 2008), but agrees with others (Lin et al. 2006, Yu et al. 2007). Part of the discrepancy between these results and previous ones may be due to the gradient of aerosol absorption properties north to south. The focus area of this study is embedded in the deforestation zone, with smoke having higher single scattering albedo (less absorption) than the smoke in the Cerrado to the south (Dubovik et al. 2002). A less absorbing smoke will have less radiative effect than the model formulated by Koren et al. (2008).

If the aerosol is affecting cloud microphysics, the signal should be apparent in the cloud optical depth (COD) as well in the cloud fraction. Fig 5a shows COD binned by AOD for four out of the five CWV groupings in Fig 4. The lowest CWV grouping is not included due to relatively large standard errors in each bin resulting from an insufficient sample size. According to the aerosol first indirect effect, increases in aerosol number loading increase the number concentration of cloud condensation nuclei, which in turn increase cloud reflectivity (Twomey 1977). This effect would be observed as an increase in COD with increasing AOD in Fig 5a. However, Fig 5a illustrates that for all CWV groupings, COD increases only to a certain AOD threshold between 0.2 and 0.3, and then decreases with increasing AOD. The highest magnitude peak in COD occurs for the lowest CWV grouping, which also

corresponds to the lowest cloud fraction from Fig 5. The lowest COD and least negative correlation with AOD corresponds to the highest CWV and largest cloud fraction. Note that Fig 5a includes clouds at all stages of vertical development, as long as the clouds are in the liquid phase.

Fig 5b also shows COD binned by AOD, but only for pixels with average cloud top pressures between 800 hPa and 850 hPa. This range is roughly between the median and mean liquid water cloud top pressures over the four year period. Fig 5b shows a similar boomerang pattern of COD versus AOD as Fig 5a, except with more noise. Only a narrow range of cloud top pressures are retained to ensure that the COD versus AOD relationships observed in Fig 5a are not merely the result of sampling clouds at different stages of growth. Even if this were the case, the addition of biomass burning aerosols has been shown to increase cloud top pressure, which would in turn likely increase COD with increasing AOD, not decrease COD as shown in Fig 5a (Koren et al. 2005, Koren et al. 2008). The AOD turning point of the boomerang occurs at generally higher AODs than in Fig 5a, specifically for the lower two CWV groupings. The magnitude of the decrease in COD with increasing AOD in terms of percentage reduction from the peak is more similar among CWV groupings than in Fig 5a. This is because in Fig 5b, all clouds have similar cloud top pressures and are situated in more homogenous cloud fields.

The increase in COD with AOD for low aerosol loading can be explained by Twomey (1977) and follows from aerosol particles affecting the microphysics of the clouds. The decrease in COD with increasing AOD above AODs of 0.3 in Fig 5a can be explained by a combination of physical processes and satellite retrieval artifacts. Physically, aerosol absorption of solar radiation can evaporate or thin the clouds optically. However, satellite retrieval artifacts can also play a role. Dark smoke above or within clouds (Kaufman and Nakajima, 1993), or subpixel holes in the clouds that reveal a dark surface beneath reduces the visible reflectance received by the satellite, and this is interpreted by the retrieval as a lower COD. In fact a physical-artificial feedback can be started in which the aerosol begins to thin the cloud via radiative processes, revealing more holes that introduce darker visible reflectance to the satellite measurements. The microphysical effect dominates at lower AODs whereas the physical and artificial effects that will decrease COD with aerosol loading are radiative in nature and will dominate at higher AODs. Considering that all explanations for COD decrease are dependent on aerosol radiative absorption, the strength of the COD decrease

should be inversely proportional to cloud fraction, because lower cloud fraction allows the aerosol greater exposure to sunlight. When the aerosol is exposed to sunlight, more aerosol translates to even higher rates of absorption and heating. The highest magnitude COD decrease occurs for the lowest CWV grouping with the lowest cloud fraction, and the lowest magnitude COD decrease occurs for the highest CWV grouping with the highest cloud fraction. Furthermore, the AOD threshold where COD changes from increasing to decreasing occurs at the lowest AOD value for the lowest CWV grouping, and the highest AOD value for the highest CWV grouping. These two patterns are consistent with the hypothesis that the COD decrease is a radiative effect of the aerosols, whether the effect is physical or artificial or a combination of both.

Sorting out the exact cause of the COD decrease with AOD is difficult. The absence of a strong absorption effect in the cloud fraction plots would suggest that darkening may play a role in the COD plots. Wilcox et al. (2009) found that biomass burning aerosols over a stratocumulus deck will artificially reduce observed cloud optical depths by the MODIS sensor (Wilcox et al. 2009). The darkening bias was found to be greater for higher AODs and also for higher non-polluted values of cloud optical depth. Both of these relationships are observed in Fig 5a. Unlike the Wilcox et al. (2009) study, the data in Fig 5 do not consist only of scenarios with aerosols above clouds. Analysis of individual days using both MODIS Aqua and the CALIPSO lidar, which has an overpass time roughly 1 minute after the Aqua satellite, results a similar boomerang trend in COD versus AOD even when the cloud layer forms at the top of the boundary layer, above the aerosols. Fig S2 shows the results of one of these days, August 12th, 2006, where clouds form above the aerosol layer and COD exhibits a boomerang trend with AOD. Colors in the Fig S2b scatter plot represent the relative uncertainty in each COD retrieval. Low COD uncertainties at high AODs suggest that the reversal in the COD trend may not be explained solely by uncertainties in the COD retrieval.

Kaufman and Nakajima (1993) also hypothesized that biomass burning aerosol darkens Amazonian clouds due to the presence of black carbon inside clouds (Kaufman and Nakajima 1993). This study found that cloud reflectance at 640 nm is reduced from 0.71 to 0.68 for an increase in aerosol optical depth between 0.1 and 2.0. This small decrease in visible reflectance (4%) is likely not the sole cause of decreases in COT between 20% and 50%, observed in Fig 5a. Because of the small role expected by the darkening of the clouds and the absence of a strong absorption effect in the cloud fraction plots, the physical-artificial

feedback involving thinning clouds and increasing inclusion of dark reflectance from the surface beneath is the most promising explanation. Modeling studies have also found that black carbon absorption in clouds results in a non-negligible feedback to surface and mid-tropospheric temperatures globally (Jacobson 2006). This in-cloud absorption may constitute up to 10% or more of the total temperature feedback from black carbon. Thus, aerosol absorption in clouds may have a large effect on the radiative balance of the atmosphere in the Amazon region.

3.2 Effect of Land-Atmosphere Interactions

Biomass burning in the Amazon affects clouds in two ways - through smoke effects and through land use changes. Smoke particles can change cloud microphysics and heat the atmospheric cloud environment by absorbing sunlight, as described above. Land use changes that convert forest to pasture and cropland change the surface heat fluxes, which also affect cloud development. By dividing our data set into forested and deforested (pasture) subsets, we can begin to understand the relative effects of aerosols and land use changes on cloud properties, and especially how land use changes modify aerosol effects.

Table 1 shows average values of cloud, aerosol, and profile parameters retrieved from the Level 2 MODIS products. Water cloud fraction is substantially higher for the pasture compared to the forest, which agrees with previous studies (Cutrim et al. 1995, Negri et al. 2004, Wang et al. 2009). In addition, a lower average cloud top pressure is observed for the pasture, which suggests more shallow cloud development over the pasture compared to the forest. This result also agrees with previous observational and modeling studies (Wang et al. 2000, Chagnon et al. 2004, Correia et al. 2007, Wang et al. 2009). A consequence of deeper warm clouds over the forest is larger average liquid water paths over the forest. Column water vapor is also higher over the forest, due to the reduction in evapotranspiration over the pasture compared to the forest (Salati and Nobre 1991). Higher atmospheric low-level stability is observed over the pasture, a parameter defined as the temperature at 850 hPa minus the temperature at 1000 hPa. The shorter roughness length and lower specific heat of the pasture result in greater surface heating, as supported by the higher 1000 hPa temperature compared to the forest. This heating is hypothesized to help spawn shallow cumulus clouds (Negri et al. 2004). The difference in low-level atmospheric stability, roughly 4 K, correlates well with other studies (Polcher and Laval 1994, Correia et al. 2007). Aerosol optical depth is almost identical between the two land cover types, as we would expect since aerosol

concentrations are often relatively spatially homogenous for hundreds of kilometers, particularly at some distance away from concentrated smoke plumes (Artaxo et al. 1998, Smirnov et al. 2000).

Comparison of aerosol effects on CWV and clouds between different land cover types requires careful consideration of consistent sampling procedures. To perform this analysis, the same number of samples must be retrieved between forest and pasture for a given day for each AOD bin to ensure that weighting of the data by time of the year is consistent between both land cover types. The sampling process is as follows: First, for each parameter and each AOD bin, the number of samples for each day is determined for forest and pasture. For the land cover type (forested or deforested) with the minimum number of samples, the same number of samples is taken from the other land cover type. Because bin edges must be assigned beforehand using this procedure, the number of samples in each AOD bin is not consistent along all bins. The eight bins for both forest and pasture are equally spaced between 0.05 and 0.8.

Several randomized mixed forest and pasture simulations are also conducted to assess the significance of the segregated land cover analysis. In each random simulation, the retrievals are randomly sampled between forest and pasture according to the relative proportion of forest and pasture retrievals in the actual data, so in effect there is no systematic segregation by land cover in each randomized simulation. Again, the data is processed such that the same number of samples is retained between forest and pasture for a given day for each AOD bin.

The black line in Fig 6a illustrates the difference in the average sampled Julian Day between pasture and forest in each AOD bin. The difference is zero for all bins, indicating that the sampling procedure by definition does not weight the result by day of the year, thus there is no difference in large-scale meteorology between the pasture and forest for each AOD bin. The red dotted lines represent the results of five randomized simulations. Again, because the algorithm does not weight the result by day of the year, there is no difference in large-scale meteorology between the forest and pasture for each AOD bin in the randomized simulations.

One of the primary underlying assumptions in this study is that aerosols do not impact CWV through changes in evaporation and transpiration, but instead that CWV is an indicator of the synoptic scale meteorology. Aerosols could, in theory, affect evapotranspiration rates by changing both the magnitude and diffuse fractionation of radiation reaching the surface (Jacobson 2002, Roderick et al. 2001, Min 2005, Knohl et al. 2008, Still et al. 2009). Because

deforested land has a leaf area index several times lower than forested land, in addition to a significantly lower heat capacity, aerosols could affect the evapotranspiration and evaporation from the ground differently between forested and deforested land. We test this assumption by analyzing aerosol-CWV relationships separately over the forested area and deforested area in Fig 1. Table 1 indicates that the forest CWV is on average 0.2 cm higher than the pasture during the dry seasons of 2004 to 2007, which we assume is the result of differences in evapotranspiration. If we observe this difference correlated with aerosol, then we know that aerosol is modifying the CWV values and our assumption of using CWV as a tracer for the large-scale meteorology is incorrect.

Fig 6b shows CWV binned by AOD over the pasture minus CWV binned by AOD over the forest, again for retrievals that also have cloud fractions above zero. Error bars represent the square root of the sum of the pasture and forest standard errors squared. Red dotted lines again represent the results of the random simulations. There is a lack of a significant trend in CWV differences with AOD. Instead, CWV is roughly 0.1 cm greater over the forest compared to the deforested land for all bins, an offset owed to the difference in evapotranspiration between pasture and forest. The random simulations show no such offset since forest and pasture retrievals are randomly mixed in these simulations. In addition, the magnitude of the variability between AOD bins is similar between the data and the random simulations, further supporting the absence of correlation between CWV and AOD.

Fig 6b shows that addition of aerosols below an AOD of 0.8 does not influence evapotranspiration sufficiently to affect CWV differently between pasture and forest. Difference values between pasture and forest do not vary greatly along AOD bins, and the little variation that does exist is well within the standard error. More generally, the addition of aerosol below an AOD of 0.8 does not have a noticeable impact on CWV. Thus, changes in CWV may be attributed completely to changes in synoptic-scale conditions.

Fig 6c shows the difference between cloud fraction binned by AOD over the pasture and over the forest. Absolute values of aerosol-cloud correlations over forest and pasture are not computed as they will be influenced by variations in CWV, similar to Fig 3. However, because the same number of retrievals is retained over the forest and pasture for each day in each AOD bin, computing cloud fraction differences between forest and pasture in each AOD bin will remove influences of the larger-scale meteorology.

The cloud fraction difference between pasture and forest is always positive in Fig 6c, indicating that cloud fraction is greater over the pasture than the forest, as suggested by Table 1. The figure also illustrates that there are increasingly more clouds over the pasture with increasing AOD, up to an AOD of 0.5. At this AOD threshold, the trend begins to flatten out, and even reverses slightly. The five random simulations do not show higher average cloud fractions over the pasture, nor do they show a stronger microphysical aerosol forcing over the pasture, supporting the significance of these results in the actual data. What causes this noticeable dissimilarity in the aerosol effect between pasture and forest at low AODs below 0.5? Because differences in CWV are likely not a driving factor due the results of Fig 6b, it is suggested that differences in low-level atmospheric stability may be at the root of the dissimilarity.

Fig 6d again shows the difference in cloud fraction binned by AOD between the pasture and forest (black line), but also shows lines representing cloud fraction difference stratified by stability. The red line includes all retrievals where the low-level stability, defined as the temperature at 850 hPa minus the temperature at 1000 hPa, is less than -16 K over the pasture and greater than -16 K over the forest. The blue line includes all retrievals where the low-level stability is greater than -16 K over the pasture and less than -16 K over the forest. This threshold stability value of -16 K is selected because it is very close to the median stability over both pasture and forest. In addition, a temperature difference of 16 K or greater between 850 and 1000 hPa conservatively corresponds to an unstable atmosphere, according to a tropical standard atmosphere **(A height of 1529 meters corresponds to 850 hPa at 15° N).**

The red line represents the difference in cloud fraction between pasture and forest only for retrievals where the pasture is considered absolutely unstable and the forest is relatively more stable. In this case (red line), the difference in cloud fraction between pasture and forest responds similarly to increasing AOD as the case that includes all stabilities (black line). This similarity is expected since the pasture is often more unstable than the forest. The blue line represents the reverse situation, retrievals where the forest is considered absolutely unstable and the pasture relatively more stable. Because this scenario is less likely, larger errors are observed. Unlike the black and red lines that show increasing clouds over the pasture with increasing AOD, the blue line does not exhibit such a trend. The absence of a trend may be attributed to the higher stability over the pasture compared to the forest – the microphysical forcing of clouds may be weaker in atmospheres that lack sufficient low-level instability.

Low level stability appears to be a factor or a tracer for how aerosol modifies cloud fraction differently over forested and deforested surfaces. The greater instability that generally occurs over pasture appears to encourage increases in cloud fraction with AOD. Yet, the response of COD to increasing AOD, when analyzed, did not appear to be substantially different between forest and pasture. The statistical approach used here is extremely limited, and cannot characterize the full mesoscale circulations thought to be responsible for the general differences in cloud fraction between forested and deforested surfaces (Wang et al. 2009). A proper 3D cloud resolving model with adequate similations of surface fluxes and mesoscale circulations will be needed to explain the associations identified in Fig 6c and Fig 6d.

4 Conclusions

In this study, a 5° NE x 5° WE region over Rondônia, Brazil was analyzed using high resolution aerosol, cloud, water vapor, and atmospheric profile data from the Moderate Resolution Imaging Spectroradiometer (MODIS). Four years of data (2004 - 2007) during the biomass burning transition season (Aug - Oct) were compiled to analyze the effect of aerosols on warm cloud development. Several years of data were employed to gather a large enough dataset for analysis, and to smooth out interannual variability. The MODIS water vapor and aerosol products illustrate that column water vapor (CWV) increased throughout the biomass burning season, while aerosol loading peaked during the middle of the season. These intraseasonal trends may produce false correlations in cloud parameter versus AOD plots when all data throughout the biomass burning season are accumulated and analyzed together. By dividing the total period into subperiods, we found evidence that both large-scale meteorological factors traced by CWV and aerosol loading contributed to modification of the cloud fraction in our area of interest. To better account for this meteorological variability, data were stratified by column water vapor. When background CWV variability was removed, cloud fraction increased with AOD, at nearly all levels of CWV, but the strongest increases occurred at the highest values of column water vapor.

Decrease of cloud fraction with AOD, attributed to aerosol absorption effects, was not observed in the cloud fraction versus AOD plots once the data were stratified by CWV. However, the decrease was seen in the data divided into seasonal subsets, and associations between cloud fraction and aerosol were consistent with expectations that follow from the aerosol-cloud fraction feedback hypothesized by Koren et al. (2008). At lower cloud

fractions when the aerosol has greater exposure to sunlight, the decrease of cloud fraction attributed to aerosol absorption effects increased in magnitude and was shifted to lower values of AOD.

Relationships between cloud optical depth and aerosol loading are more difficult to interpret. Plots of COD against AOD showed an initial increase of cloud optical thickness, and then a turning point where clouds appeared to become optically thinner as aerosols increased. Increasing COD with aerosol can be attributed physically to the processes described by Twomey (1977), but the decrease of COD with AOD is best described by a combination of physical processes and satellite retrieval artifacts. Absorbing aerosol may cause cloud droplets to evaporate and clouds to thin. This is a legitimate physical process. On the other hand, the dark aerosol in and above the cloud may also decrease the cloud reflectance observed by the satellite, which the satellite retrieval interprets as a decrease in COD. As the cloud thins, subpixel holes in the cloud open, allowing darker reflectance from the surface beneath to again darken the cloud reflectance measured by the satellite. Again the cloud reflectance is artificially too low, resulting in COD retrievals that are too low, which contributes to the strong decrease of COD with AOD observed in the data analysis. Assuming that the decreasing trend in COD with AOD is due to both radiative effects as well as retrieval artifacts, our results suggest that GCMs that do not include treatment of aerosol absorption in clouds are inaccurate over regions with high concentrations of absorbing aerosol.

This study also addressed the effect of aerosols on CWV and clouds over different land cover types. Land cover was segregated into forested and deforested groupings using the MODIS land cover product, and the response of CWV to increasing AOD was analyzed between the forested and deforested land. We found that aerosols do not have a noticeable effect on CWV. Thus, it can be assumed that temporal changes in CWV are largely a function of the synoptic-scale meteorology and that aerosol is completely independent of the column water vapor at the local level. The independence of CWV and AOD is an inherent assumption in the former portion of the paper, supported by the analysis in the latter portion of the paper.

This study showed that the *relationship* between cloud fraction and AOD is quite sensitive to land cover type. Microphysical effects appeared to be stronger over the deforested land compared to the forested land, increasing cloud fraction with AOD to a greater extent over the deforested land compared to the forest. The difference in the aerosol microphysical effect

over forested and deforested land appears to be linked to the differing lower tropospheric stability over these two surfaces, but a full understanding of the complex interaction between aerosols, clouds and surface types cannot be achieved from the statistical approach used here. A 3D cloud resolving model with adequate representation of surface-atmosphere exchange and ability to similate mesoscale circulations and cloud microphysical processes will be required.

The relationships shown here cannot, with certainty, be extrapolated to different times of the year or different regions of the world. These aerosol-cloud correlations are largely dependent on the physical and optical characteristics of the biomass burning aerosol (i.e. size distribution, composition); therefore a different aerosol mixture may or may not have a different impact on clouds. However, a similar analysis to this one over other biomass burning regions or heavily fossil-fuel polluted regions would be helpful in determining if these relationships could be extended more generally. More importantly, modeling-based studies are required to assign causation to the correlations found here.

Acknowledgements

This study was supported by NASA grant NNX07AN25G as well as the NASA Earth Systems Science Fellowship and the Stanford Graduate Fellowship. We are grateful to Steven Platnick, Steven Ackerman, and Rich Kleidman for helpful comments. We also thank the Brent Holben and his staff for establishing and maintaining the two AERONET sites used in this investigation, Abracos Hill and Ji Paraná SE.

References

Ackerman, A. S., Toon, O. B., Stevens, D. E., Heymsfield, A. J., Ramanathan, V., and Welton, E. J.: Reduction of tropical cloudiness by soot, Science, 288, 2000.

Ackerman, A. S., Strabala, K. I., Menzel, W. P., Frey, R. A., Moeller, C. C., and Gumley, L. E.: Discriminating clear sky from clouds with MODIS, J. Geophys. Res., 103(D24), 32141 - 32157, 1998.

1 Ackerman, A. S., Strabala, K. I., Menzel, W. P., Frey, R. A., Moeller, C. C., Gumley, L. E.,
2 Baum, B., Schaff, C., and Riggs, G.: Discriminating clear sky from clouds with MODIS -
3 Algorithm Theoretical Basis Document, NASA Goddard Space Flight Center, 1997.

4 Albrecht, B. A.: Aerosols, cloud microphysics, and fractional cloudiness, Science, 245, 1227-
5 1230, 1989.

6 Andreae, M. O. et al.: Biogeochemical cycling of carbon, water, energy, trace gases, and
7 aerosols in Amazonia: The LBA-EUSTACH experiments, J. Geophys. Res., 107(D20), 8066,
8 2002.

9 Andreae, M. O., Rosenfeld, D., Artaxo, P., Costa, A. A., Frank, G. P., Longo, K. M., and
10 Silva-Dias, M. A. F.: Smoking rain clouds over the Amazon, Science, 303, 1337-1342, 2004.

11 Artaxo, P., Fernandas, E. T., Martins, J. V., Yamasoe, M. A., Hobbs., P. V., Maenhaut, W.,
12 Longo, K. M., and Castanho, A.: Large-scale aerosol source apportionment in Amazonia, J.
13 Geophys. Res., 103(D24), 31837-31847, 1998.

14 Brennan, J. I., Kaufman, Y. J., Koren, I., and Li, R.-R: Aerosol-cloud interaction –
15 misclassification of MODIS clouds in heavy aerosol, IEEE T. Geosci. Remote, 43(4), 911-
16 915, 2005.

17 Chand, D., Wood, R., Anderson, T. L., Satheesh, S. K., and Charlson, R. J.: Satellite-derived
18 direct radiative effect of aerosols dependent on cloud clover, Nature Geosci., 2, 181 – 184,
19 2009.

20 Chagnon, F. J. F., Bras, R. L. and Wang, J.: Climatic shift in patterns of shallow clouds over
21 the Amazon, Geophys. Res. Lett., 31, L24212, 2004.

22 Correia, F. W. S., Alvalá, R. C. S., and Manzi, A. O.: Modeling the impacts of land cover
23 change in Amazonia: a regional climate model (RCM) simulation study, Theor. Appl.
24 Climatol., 93, 225-244, 2007.

25 Cutrim, E., Marin, D. W., and Rabin, R.: Enhancement of cumulus clouds over deforested
26 lands in Amazonia, B. Am. Meteorol. Soc., 76, 1801-1805, 1995.

27 Davidi, A., Koren, I., and Remer, L.: Direct measurements of the effect of biomass burning
28 over the Amazon on the atmospheric temperature profile. Atmos. Chem. Phys., 9, 8211-8221,
29 2009.

1 D'Almeida, C., C. J. Vorosmarty, Hurtt, G. C., Marengo, J. A., Dingman, S. L., and Keim, B.
2 D.: The effects of deforestation on the hydrological cycle in Amazonia: a review on scale and
3 resolution, Int. J. Climatol., 27, 633-647, 2007.

4 Diner, D. J., et al.: Multi-angle Imaging SpectroRadiometer (MISR) instrument description
5 and experiment overview, IEEE T. Geosci. Remote, 36(4), 1072-1087, 1998.

6 Dubovik, O., Holben, B. N., Eck. T. F., Smirnov, A., Kaufman, Y. J., King, M. D., Tanré, D.,
7 and Slutsker, I.: Variability of absorption and optical properties of key aerosol types observed
8 in worldwide locations. J. Atmos. Sci., 59, 590-608, 2002.

9 Feingold, G., Remer, L. A., Ramaprasad, J., and Kaufman, Y. J.: Analysis of smoke impacts
10 on clouds in Brazilian biomass burning regions: an extension of Twomey's approach, J.
11 Geophys. Res., 106(D19), 22907-22922, 2001.

12 Feingold, G., Jiang, H, and Harrington, J. Y.: On smoke suppression of clouds in Amazonia,
13 Geophys. Res. Lett., 32, L02840, 2005.

14 Gao, B.-C., and Kaufman, Y. J.: The MODIS near-IR water vapor algorithm - Algorithm
15 Theoretical Basis Document, NASA Goddard Space Flight Center, 1998.

16 Gunn, R. and Phillips, B. B.: An experimental investigation of the effect of air pollution on
17 the initiation of rain, J. Meteorol., 14, 272-280, 1957.

18 Henderson-Sellers, A., and Gornitz, V.: Possible climatic impacts of land cover
19 transformations, with particular emphasis on tropical deforestation, Climatic Change, 6, 231-
20 257, 1984.

21 Holben, B. N., et al.: AERONET – A federated instrument network and data archive for
22 aerosol characterization, Remote Sens. Environ., 66, 1-16, 1998.

23 Jacobson, M. Z.: Control of fossil-fuel particulate black carbon and organic matter, possibly
24 the most effective method of slowing global warming, J. Geophys. Res., 107(D19), 4410,
25 2002.

26 Jacobson, M. Z.: Effects of externally-through-internally-mixed soot inclusions within clouds
27 and precipitation on global climate, J. Phys. Chem. A., 110(21), 6860-6873, 2006.

28 Kalnay, E., et al.: The NCEP/NCAR 40-Year Reanalysis Project. B. Am. Meteorol. Soc., 77,
29 437-471, 1996.

Kaufman, Y. J., and Fraser, R. S.: The effect of smoke particles on clouds and climate forcing, Science, 277, 1636-1639, 1997.

Kaufman, Y. J., and Koren, I.: Smoke and pollution aerosol effect on cloud cover, Science, 313, 655-658, 2006.

Kaufman, Y. J., and Nakajima, T.: Effect of Amazon smoke on cloud microphysics and albedo – analysis from satellite imagery, J. App. Meteorol., 32, 729-744, 1993.

Kaufman, Y. J., Koren, I., Remer, L. A., Rosenfeld, D., and Rudich, Y.: The effect of smoke, dust, and pollution aerosol on shallow cloud development over the Atlantic Ocean, Proc. Natl. Acad. Sci., 102(32), 11207-11212, 2005a.

Kaufman, Y. J., Remer, L. A., Tanré, D., Li, R.–R., Kleidman, R., Matoo, S., Levy, R., Eck, T. M., Holben, B. N., Ichoku, C., Martins, J. V., and Koren, I.: A critical examination of the residual cloud contamination and diurnal sampling effects on MODIS estimates of aerosol over ocean, IEEE T. Geosci. Remote, 43(12), 2886-2897, 2005b.

Kaufman, Y. J., Tanré, D., and Boucher, O.: A satellite view of aerosols in the climate system, Nature, 419, 215-223, 2002.

Kaufman, Y. J., Tanré, D., Remer, L. A., Vermote, E. F., Chu, A., and Holben, B. N.: Operational remote sensing of tropospheric aerosol over the land from EOS Moderate Resolution Imaging Spectroradiometer, J. Geophys. Res., 102(D14), 17051-17067, 1997.

Khain, A., Rosenfeld, D., and Pokrovsky, A.: Aerosol impact on the dynamics and microphysics of deep convective clouds, Q. J. R. Meteorol. Soc., 131, 2639-2663, 2005.

King, M. D., Menzel, W. P., Kaufman, Y. J., Tanré, D., Gao, B.-C., Platnick, S., Ackerman, S. A., Remer, L. A., Pincus, R., and Hubanks, P. A.: Cloud and aerosol properties, precipitable water, and profiles of temperature and humidity from MODIS, IEEE T. Geosci. Remote, 41(2), 442-458, 2003.

King, M. D., Tsay, S.-C., Platnick, S., Wang, M., and Liou, K.-N.: Cloud retrieval algorithms for MODIS: Optical thickness, effective particle radius, and thermodynamic phase – Algorithm Theoretical Basis Document, NASA Goddard Space Flight Center, 1997.

Knohl, A. and Baldocchi, D. D.: Effects of diffuse radiation on canopy gas exchange processes in a forest ecosystem, J. Geophys. Res., 113, G02023, 2008.

Koren, I., Kaufman, Y. J., Remer, L. A., and Martins, J. V.: Measurement of the effect of Amazon smoke on inhibition of cloud formation, Science, 303, 1342-1345, 2004.

Koren, I., Kaufman, Y. J., Rosenfeld, D., Remer, L. A., and Rudich, Y.: Aerosol invigoration and restructuring of Atlantic convective clouds, Geophys. Res. Lett., 32, L14828, 2005.

Koren, I., Martins, J. V., Remer, L. A., and Afargan, H.: Smoke invigoration versus inhibition of clouds over the Amazon, Science, 321, 946-949, 2008.

Koren, I., Remer, L. A., and Longo, K.: Reversal of trend of biomass burning in the Amazon, Geophys. Res. Lett., 34, L20404, 2007.

Levy, R. C., Remer, L. A., Mattoo, S., Vermote, E. F., and Kaufman, Y. J.: Second-generation operation algorithm: Retrieval of aerosol properties over land from inversion of Moderate Resolution Imaging Spectroradiometer spectral reflectance, J. Geophys. Res., 112, D13211, 2007.

Lin, J. C., Matsui, T., Pielke Sr., R. A., and Kummerow, C.: Effects of biomass-burning-derived aerosols on precipitation and clouds in the Amazon Basin: a satellite-based empirical study, J. Geophys. Res., 111, D19204, 2006.

Marques, J., dos Santos, J. M., Villa Nova, N. A. and Salati, E.: Precipitable water and water vapor flux between Belém and Manaus, Acta Amazônica, 7(3), 355-362, 1977.

Martins, J. A., Silva Dias, M. A. F., and Gonçalves, F. L. T.: Impact of biomass burning aerosols on precipitation in the Amazon: a modeling case study, J. Geophys. Res., 114, D02207, 2009.

Meskhidze, N., Remer, L. A., Platnick, S., Negrón Juárez, R., Lichtenberger, M., and Aiyyer, A. R.: Exploring the differences in cloud properties observed by the Terra and Aqua MODIS sensors, Atmos. Chem. Phys., 9, 2461-2475, 2009.

Min, Q.: Impacts of aerosols and clouds on forest-atmosphere carbon exchange, J. Geophys. Res., 110, D06203, 2005.

Myhre, G., Stordal, F., Johnsrud, J., Kaufman, Y. J., Rosenfeld, D., Storelvmo, T., Kristjansson, J. E., Berntsen, T. K., Myhre, A., and Isaksen., I. S. A.: Aerosol-cloud interaction inferred from MODIS satellite data and global aerosol models, Atmos. Chem. Phys., 7, 3081-3101, 2007.

1 Nakajima, T., and King, M. D.: Determination of the optical thickness and effective particle
2 radius of clouds from reflected solar radiation measurements, Part I: Theory, J. Atmos. Sci.,
3 47, 1878-1893, 1990.

4 Nakajima, T., King, M. D., Spinhirne, J. D., and Radke, L. F.: Determination of the optical
5 thickness and effective particle radius of clouds from reflected solar radiation measurements,
6 Part II: Marine stratocumulus observations, J. Atmos. Sci., 48, 728-751, 1991.

7 Negri, A. J., Adler, R. F., Xu, L., and Surratt, J.: The impact of Amazonian deforestation on
8 dry season rainfall, J. Climate, 17, 1306-1319, 2004.

9 Nobre, C. A., Mattos, L. F., Dereczynski, C. P., Tarasova, T. A., and Trosnikov, I. V.:
10 Overview of atmospheric conditions during the Smoke, Clouds and Radiation-Brazil (SCAR-
11 B) field experiment, J. Geophys. Res., 103(D24), 31809-31820, 1998.

12 Nobre, C. A., Sellers, P. J., and Shukla, J.: Amazonian deforestation and regional climate
13 change, J. Climate, 4, 957-988, 1991.

14 Platnick, S., King, M. D., Ackerman, S. A., Menzel, W. P., Baum, B. A., and Riedi, J. C.: The
15 MODIS cloud products: Algorithms and examples from Terra, IEEE T. Geosci. Remote,
16 41(2), 459-473, 2003.

17 Polcher, J., and Laval, K.: The impact of African and Amazonian deforestation on tropical
18 climate, J. Hydrology (Amsterdam), 155, 389-405, 1994.

19 Reid, J. S., Hobbs, P. V., Rangno, A. L., and Hegg, D. A.: Relationships between cloud
20 droplet effective radius, liquid water content, and droplet concentration for warm clouds in
21 Brazil embedded in biomass smoke, J. Geophys. Res., 104(D6), 6145-5153, 1999.

22 Ramanathan, V., Chung, C., Kim, D., Bettge, T., Buja, L., Kiehl, J. T., Washington, W. M.,
23 Fu, Q., Sikka, D. R., Wild. M.: Atmospheric brown clouds: Impacts on South Asian climate
24 and hydrological cycle, Proc. Natl. Acad. Sci., 102(15), 5326-5333, 2005.

25 Remer, L. A., Kaufman, Y. J., Holben, B. N., Thompson, A. M., and McNamara, D.: Biomass
26 burning aerosol size distribution and modeled optical properties, J. Geophys. Res., 103(D24),
27 31879-31891, 1998.

28 Remer, L. A., Kaufman, Y. J., Tanré, D., Matoo, S., Chu, D. A., Martins, J. V., Li, R.-R.,
29 Ichoku, C., Levy, R. C., Kleidman, R. G., Eck, T. F., Vermote, E., and Holben, B. N.: The
30 MODIS aerosol algorithm, products and validation, J. Atmos. Sci., 62, 947-973, 2005.

Rosenfeld, D., Lohmann, U., Raga, G. B., O'Dowd, C. D., Kulmala, M., Fuzzi, S., Reissell, A., and Andreae, M. O.: Flood or drought: How do aerosols affect precipitation?, Science, 321, 1309-1313, 2008.

Roderick, M. L., Farquhar, G. D., Berry, S. L., and Noble, I. R.: On the direct effect of clouds and atmospheric particles on the productivity and structure of vegetation, Oecologia, 129, 21–30, 2001.

Roy, S. B., and Avissar, R.: Impact of land use/land cover change on regional hydrometeorology in Amazonia, J. Geophys. Res., 107(D20), 8037, 2002.

Salati, E., and Nobre, C A.: Possible climatic impacts of tropical deforestation, Climatic Change, 19, 177-196, 1991.

Salomonson, V. V., Barnes, W. L., Maymon, P. W., Montgomery, H. E., and Ostrow, H.: MODIS - Advanced facility instrument for studies of the Earth as a system, IEEE T. Geosci. Remote, 27, 145-153, 1989.

Seemann, S., Borbas, E. E., Li, J., Menzel, P., and Gumley, L. E.: MODIS atmospheric profile retrieval – Algorithm Theoretical Basis Document, Cooperative Institute for Meteorological Satellite Studies, University of Wisconsin, 2006.

Segal, M., Avissar, R, McCumber, M. C., and Pielke, R. A.: Evaluation of vegetation effects on the generation and modification of mesoscale circulations, J. Atmos. Sci., 45, 2268-2293, 1988.

Smirnov, A., Holben, B. N., Eck, T. F., Dubovik, O., and Slutsker, I.: Cloud-screening and quality control algorithms for the AERONET database, Remote Sens. Environ., 73(3), 337-349, 2000.

Squires, P.: The microstructure and colloidal stability of warm clouds, Part I. The relation between structure and stability, Tellus, 10, 256–271, 1958.

Still, C. J., Riley, W. J., Biraud, S. C., Noone, D. C., Buenning, N. H., Randerson, J. T., Torn, M. S., Welker, J., White, J. W. C., Vachon, R., Farquhar, G. D., and Berry, J. A.: Influence of clouds and diffuse radiation on ecosystem-atmosphere CO_2 and $CO^{18}O$ exchanges, J. Geophys. Res., 114, G01018, 2009.

Strahler, A., Muchoney, D., Borak, J., Friedl, M., Gopal, S., Lambin, E., and Moody, A., MODIS land cover and land-cover change – Algorithm Theoretical Basis Document, Department of Geography, Boston University, 1999.

Twomey, S., The influence of pollution on the shortwave albedo of clouds, J. Atmos. Sci., 34, 1149-1152, 1977.

Twomey, S., and Cocks, T.: Spectral reflectance of clouds in the near-infrared: Comparison of measurements and calculations, J. Meteor. Soc. Japan, 60, 583-592, 1982.

Twomey, S., and Cocks, T.: Remote sensing of cloud parameters from spectral reflectance in the near-infrared, Beitr. Phys. Atmos., 62, 172-179, 1989.

Yu, H., Fu, R., Dickinson, R. E., Zhang, Y., Chen, M., and Wang, H.: Interannual variability of smoke and warm cloud relationships in the Amazon as inferred from MODIS retrievals, Remote Sens. Environ., 111, 435-449, 2007.

Wang, J., Bras, R. L., and Eltahir, E. A. B.: The impact of observed deforestation on the mesoscale distribution of rainfall and clouds in Amazonia, J. Hydrometeorol., 1, 267-286, 2000.

Wang, J., Chagnon, F. J. F, Williams, E. R., Betts, A. K., Renno, N. O., Machado, L. A. T., Bisht, G., Knox, R., and Bras, R. L.: Impact of deforestation in the Amazon basin on cloud climatology, Proc. Natl. Acad. Sci., 106(10), 2670-2674, 2009.

Wen, G., Marshak, A., and Cahalan, R. F.: Impact of 3D clouds on clear sky reflectance and aerosol retrieval in a biomass burning region of Brazil, IEEE Geosci. Remote S., 3, 169-172, 2006.

Wilcox, E. M., Harshvardhan, and Platnick, S.: Estimate of the impact of absorbing aerosol over cloud on the MODIS retrievals of cloud optical thickness and effective radius using two independent retrievals of liquid water path, J. Geophys. Res., 114, D05210, 2009.

Williams, E., et al.: Contrasting convective regimes over the Amazon: Implications for cloud electrification, J. Geophys. Res., 107(D20), 8082, 2002.

Yu, H., Liu, S. C., and Dickinson, R. E.: Radiative effects of aerosols on the evolution of the atmospheric boundary layer, J. Geophys. Res., 107(D12), 4142, 2002.

Zhang, Y., Fu, R., Yu, H., Dickinson, R. E., Juarez, R. N., Chin, M., and Wang, H.: A regional climate model study of how biomass burning aerosol impacts land-atmosphere interactions over the Amazon, J. Geophys. Res., 113, D14S15, 2008.

Table 1. Average cloud and atmospheric profile statistics for all warm cloud retrievals for both forested and deforested land in the study region. The averaging period is for August through October for the years 2004, 2005, 2006, and 2007.

	Forest	**Deforested**
Cloud Effective Radius (um)	15.9	14.7
Cloud Optical Depth (-)	8.95	8.07
Cloud Fraction (-)	0.52	0.63
Cloud Top Pressure (hPa)	796.4	817.9
Cloud Water Path (g/m^2)	81.3	68.0
Column Water Vapor (cm)	3.76	3.54
850 hPa Temperature (K)	292.6	293.0
1000 hPa Temperature (K)	307.2	311.4
Low-Level Stability (Temperature 850 hPa minus Temperature 1000 hPa (K))	-14.6	-18.4
AOD at 550 nm (-)	0.92	0.89

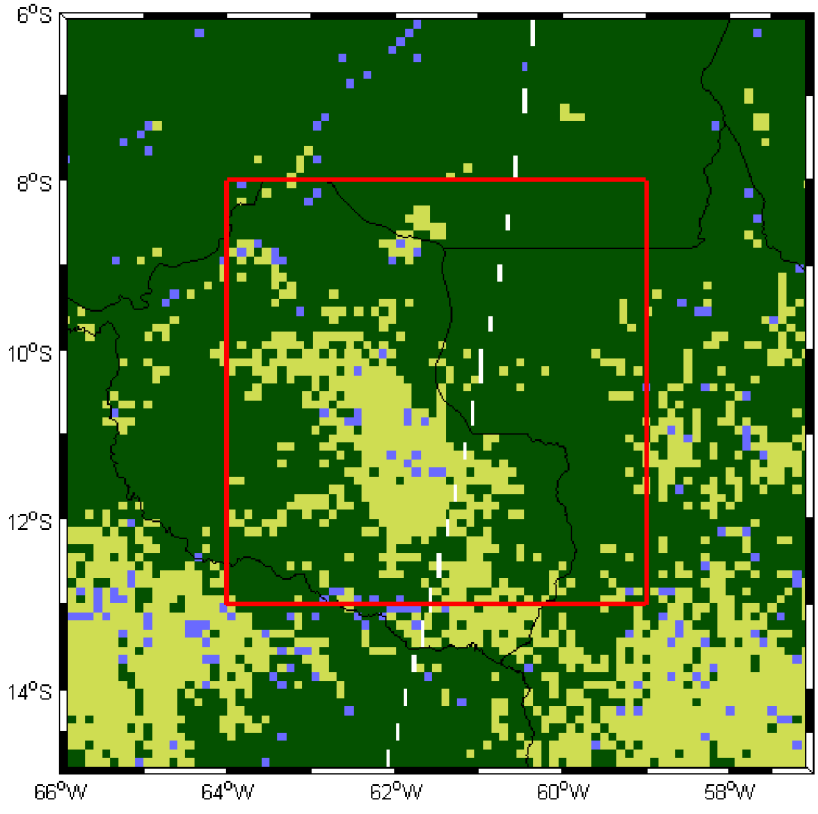

Figure 1. Land cover classifications for the year 2004. Green pixels represent evergreen forests and yellow pixels represent pasture or deforested land. Blue pixels represent land classifications that were not included in either of these two categories. The 5˚ x 5˚ study region is outlined with a red box.

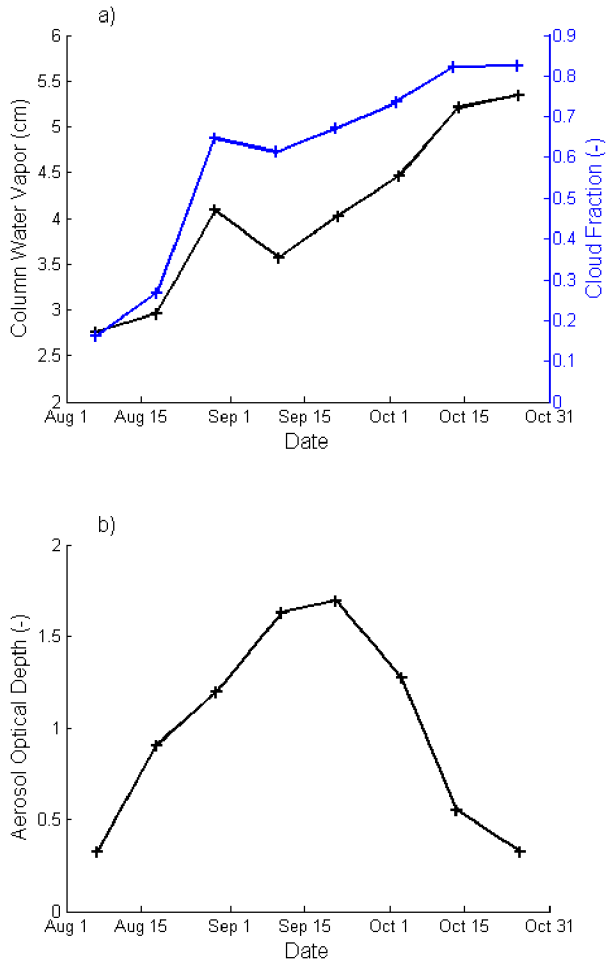

1

2 Figure 2. (a) Column water vapor and cloud fraction binned by day of the year for the months
3 of August through October, for the years 2004, 2005, 2006, and 2007. Aerosol optical depth
4 at 550 nm binned by day of the year for the same time period as in (a). Data are accumulated
5 into eight bins of equal width between August 1st and October 31st.

6

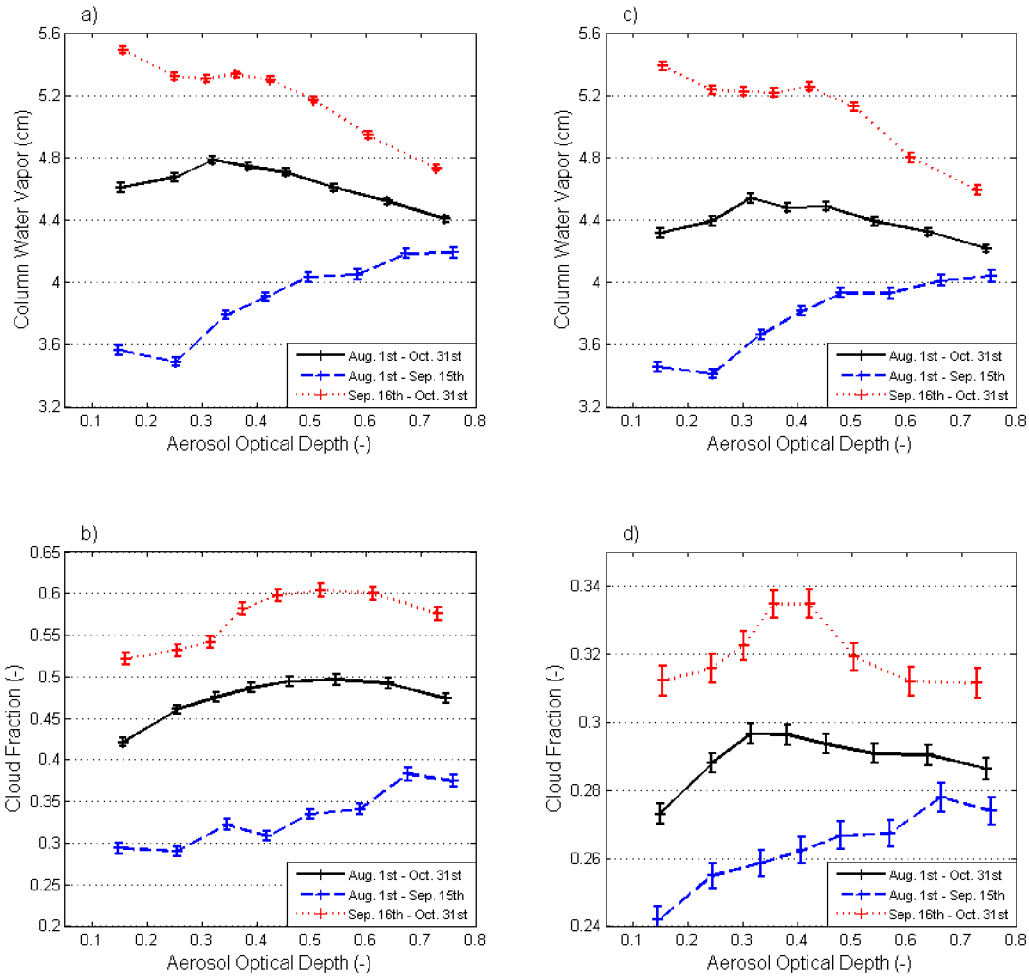

Figure 3. (a) Column water vapor binned by aerosol optical depth for all co-located warm cloud retrievals for the months of August to October, for the years 2004, 2005, 2006, and 2007. Error bars denote the standard error in each bin. (b) Cloud fraction binned by aerosol optical depth for all warm cloud retrievals for the same time period as in (a). (c) Column water vapor binned by aerosol optical depth for all co-located warm cloud retrievals with cloud fractions less than 0.5. (d) Cloud fraction binned by aerosol optical depth for all warm cloud retrievals with cloud fractions below 0.5.

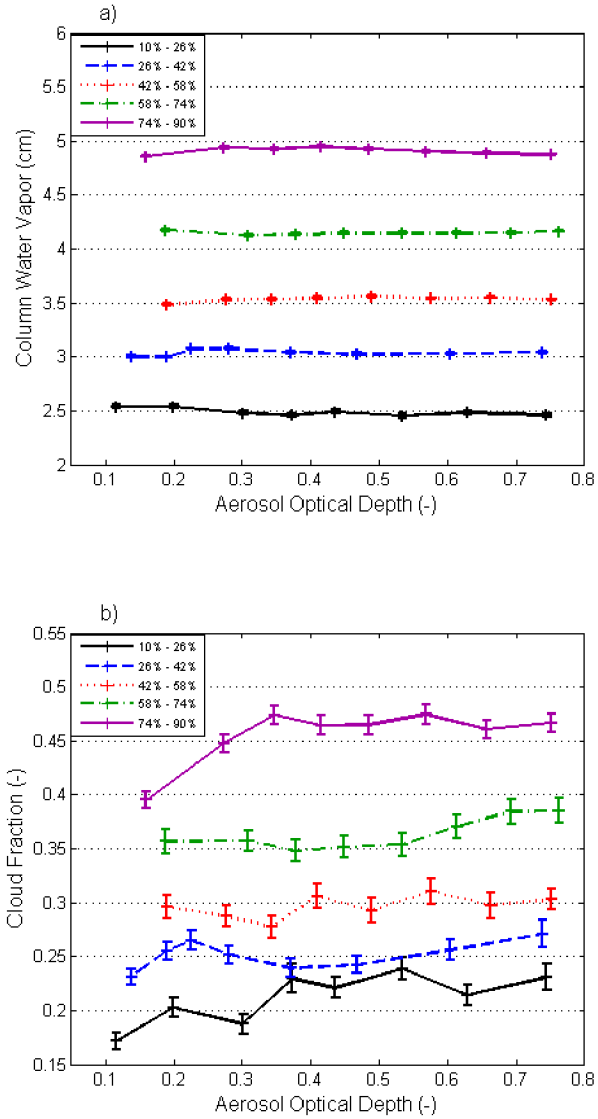

1

2 Figure 4. (a) Column water vapor binned by aerosol optical depth for all co-located warm
3 cloud retrievals at varying percentiles of column water vapor for the months of August to
4 October, for the years 2004, 2005, 2006, 2007. (b) Cloud fraction binned by aerosol optical
5 depth for all warm cloud retrievals for the same time period is in (a).

6

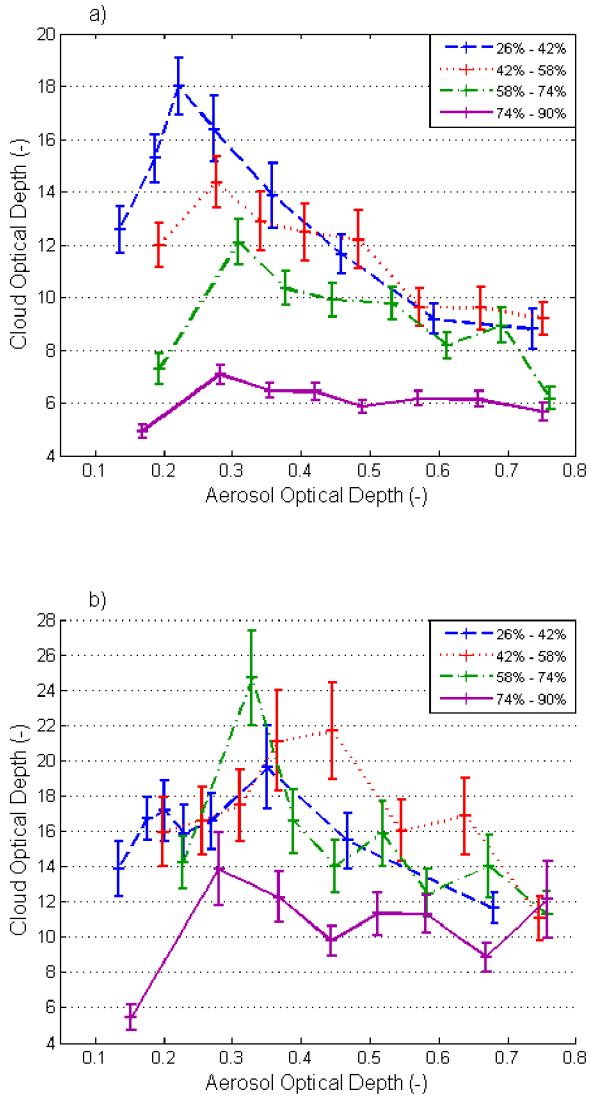

Figure 5. (a) Cloud optical depth binned by aerosol optical depth for all warm cloud retrievals at varying percentiles of column water vapor for the months of August to October, for the years 2004, 2005, 2006 and 2007. (b) Same as (a) but only for retrievals with cloud top pressures between 800 hPa and 850 hPa.

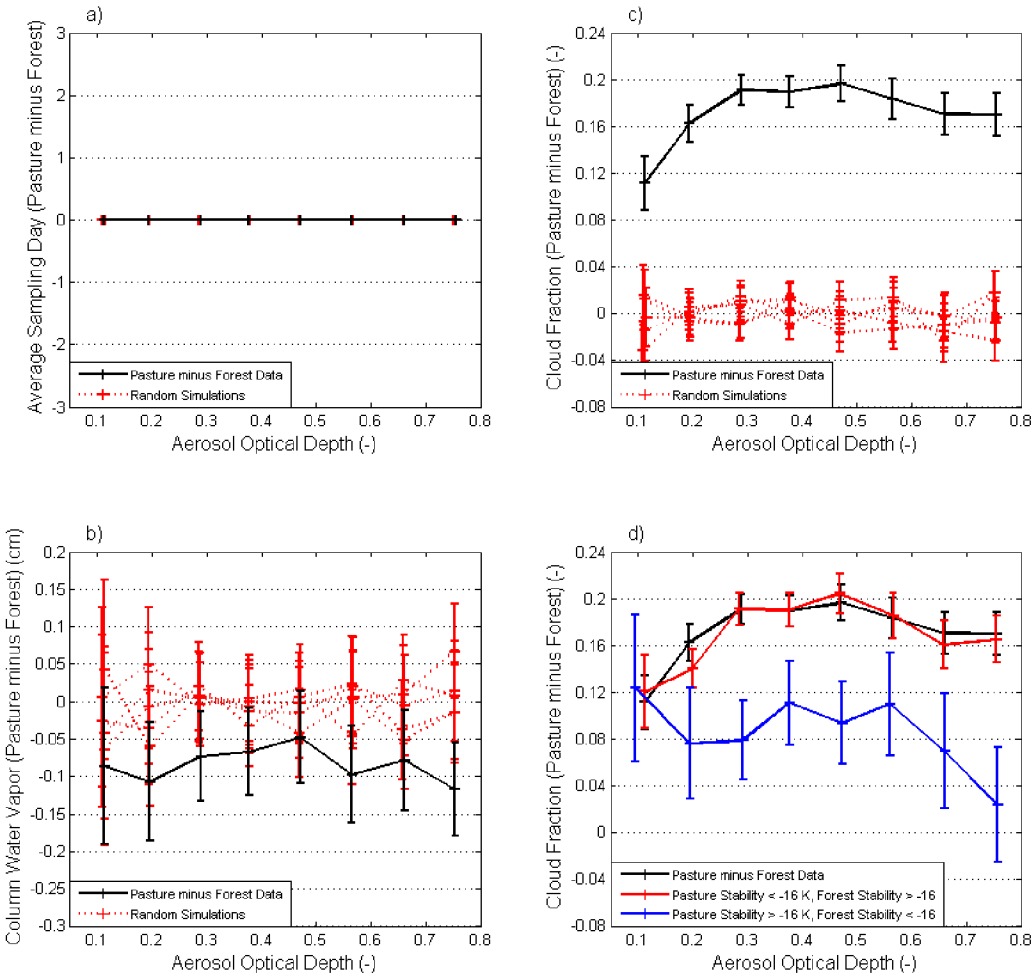

Figure 6. (a) Difference between the average sampled day of the year in each aerosol bin for the pasture and forest sites. The sampling algorithm ensures that the same number of samples per day is used from each land cover type in each AOD bin. In panels a, b and c, red lines represent the results of five random simulations, where forest and pasture pixels are mixed. Data represent the months August to October, for the years 2004 to 2007. (b) Differenced column water vapor between pasture and forest land cover types binned by AOD. (c) Differenced cloud fraction between pasture and forest land cover types binned by AOD. (d) Black line: same as (c), red and blue lines: Stratification by low level stability, defined as the temperature at 850 hPa minus the temperature at 1000 hPa. The stratification values are different between pasture and forest for each stratification case.

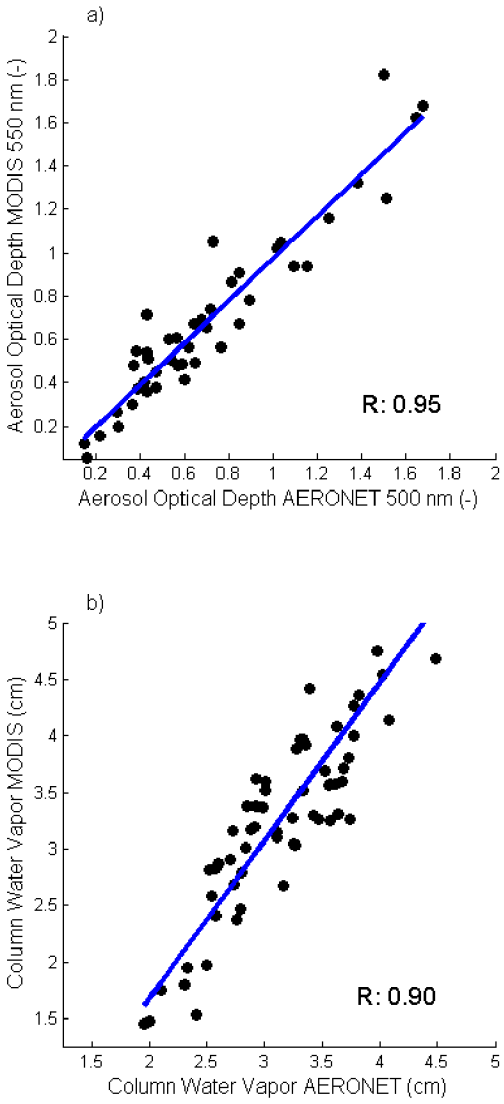

Figure S1. (a) Comparison of co-located MODIS AOD retrievals with automatic sun/sky radiometers of the Aerosol Robotic Network (AERONET) at Abracos Hill (62.358° W, 10.760° S) and Ji Paraná SE (61.852° W, 10.934° S) for days used in the study between the years 2004 through 2007 during the months of August through October. These two sites are within our 5° x 5° study region. (b) Comparison of co-located MODIS CWV retrievals with automatic AERONET retrievals for the same time period as in (a). Correlation coefficients between MODIS and AERONET data are also included in each plot.

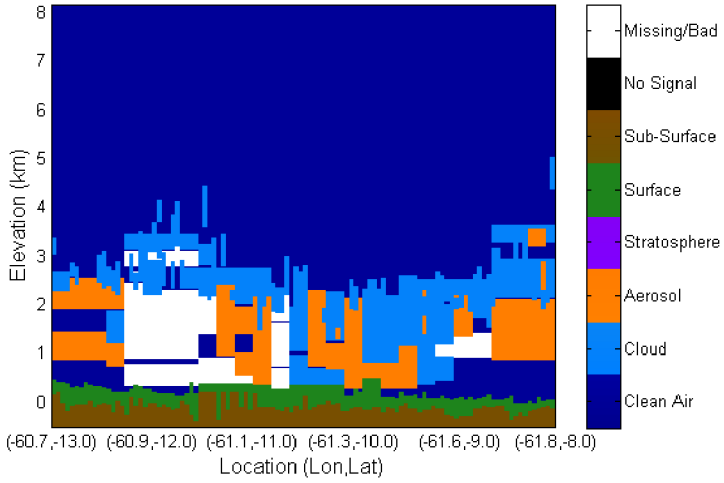

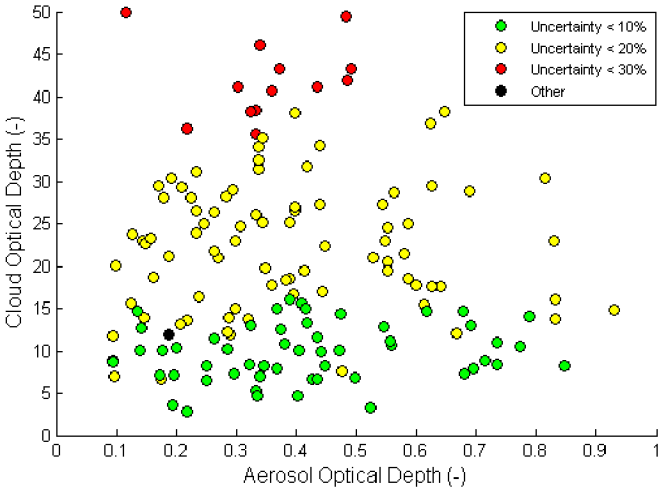

1

2 Figure S2. (a) Vertical Feature Mask from the CALIPSO lidar on a path through the study
3 region for a single day during the study period, August 12th, 2006. On this day, clouds mostly
4 form near the top of the aerosol layer. Clouds that extend throughout the column may be
5 misclassified heavy aerosol plumes. (b) Scatter plot of cloud optical depth versus aerosol
6 optical depth on the same day as (a), throughout the 5° x 5° study region. Colors correspond
7 to the cloud optical depth uncertainty parameter, defined as a percentage of the retrieved
8 value.